



A study of ion-dynamics and correlation effects for spectral line broadening in plasma: K-shell lines

E. Stambulchik*, Y. Maron

Faculty of Physics, Weizmann Institute of Science, Rehovot 76100, Israel

Accepted 26 April 2005

Abstract

A method for the calculation of spectral line broadening in plasma has been developed and implemented. The method is based on a numerical simulation of the motion of the interacting plasma particles (both ions and electrons) and the use of the resulting time-dependent field to obtain the evolution of the radiator system. The Fourier transform of the resulting radiator time-dependent dipole function then gives the spectral line shape. This approach thus naturally accounts for all frequency regions of the plasma-particle fields and for the effects of the particle interactions on the fields. Due to a rather general approach used for solving the Schrödinger equation, the method is applicable to line-shape calculations of isolated and overlapping spectral lines involving both dipole-allowed and dipole-forbidden radiative transitions. In addition, line shapes under a simultaneous influence of externally-applied (constant or time-dependent) electric and magnetic fields can be calculated in a self-consistent manner, and polarization properties of the emitted light, caused by such external fields, can be investigated. Part of the method capabilities is demonstrated. Results presented are for spectral lines of H- and He-like ions of C, Si, and Ar in non-magnetized plasmas. It is found that ion dynamics contributes to the line broadening significantly, in several cases exceeding the electron impact widths by a few times. Also, the interactions between the radiator and the perturbers cause a significant reduction in the line widths, even for overall-weakly-coupled plasmas; a relation between this effect and the radiator–perturber coupling is made.

© 2005 Elsevier Ltd. All rights reserved.

Keywords: Stark effect; Ion dynamics; Spectral line broadening

*Corresponding author.

E-mail address: Evgeny.Stambulchik@weizmann.ac.il (E. Stambulchik).

1. Introduction

Measurements of emission and absorption spectra of atoms and ions are one of the most important tools in plasma diagnostics [1]. They allow for non-intrusive diagnostics of the properties of plasmas and electromagnetic fields in various laboratory and space plasmas. In particular, spectral line shapes may be analyzed to yield a wealth of information on the plasma parameters provided, however, that the data are compared to accurate computations of the spectral line broadening with and without externally-applied electric and magnetic fields.

The modern theory of spectral line broadening in plasmas was developed in the 1960s [2–4]. In the theory, the effects of the plasma environment on the emission spectrum is split into two parts characterized by two radically different frequency regions. The ions are essentially stationary and their effect is that of a static Stark effect, with the broadening caused by an averaging over all possible fields corresponding to the different ion configurations near the perturbed atom or ion (the quasistatic approximation). For each of the ion-field configurations, the effect of electrons has then to be calculated. The electrons, because of their high mobility, perturb the radiator by means of “collisions”. These collisions cause a change of the radiator state, thus interrupting the spontaneous radiation, or alter the energy levels of the radiator, which results in a phase shift (the impact approximation). The net effect of these processes, averaged over the time and number of radiators, gives the spectral line broadening and shift.

Traditionally, ion effects in most cases were calculated within the quasistatic approximation, while the electron perturbation was believed to satisfy the impact approximation. The formal description of the method is given by the following formula:

$$I(\omega) = \frac{1}{\pi} \Re \text{Tr} \int_0^\infty dF W(F) \{ \Delta_d [i\omega - i\omega(F) + \phi(F)]^{-1} \}, \quad (1)$$

where $W(F)$ is the ion microfield distribution function, Δ_d is the dipole–dipole operator, $\omega(F)$ is the quasistatic Stark shift of the level energy, and ϕ is the so-called impact operator that, in general, depends on the ion field F . This approach to Stark line-broadening is commonly referred to as the “Standard Theory” (ST).

This separation of perturbations into ion and electron parts, in general, cannot be made without a loss of accuracy, although it is argued [5] that in many cases it is justified. A more serious problem, however, is that each of the ion and electron parts often needs to be considered beyond the limits of the quasistatic and impact approximations. In particular, the ion motion in plasma leads to the so-called ion dynamics effects. It was first shown theoretically [6,7] and soon found in experiments [8–10], that the ion dynamics can be responsible for significant corrections to the spectral line widths.

In order to advance the calculations beyond the ST, several computer simulation methods have been developed (for a comprehensive review of the development in the field since the ST foundation, see Ref. [1]). Among the first is the work described in Ref. [11], where a computer code was used to simulate the ion motion along straight paths, while the electron contribution was still calculated using the impact approximation. The method was further improved [12] by using molecular-dynamics (MD) simulations for the ions, thus accounting for interactions between the radiators and the ion perturbers. Then, more improvements were developed [13–16], where the motion of both ions and electrons was numerically simulated, resulting in a correct treatment of the intermediate time scales of the electric-field fluctuations. The particle motion was simulated

using straight path trajectories, which is applicable to cases of neutral radiators or, in general, when the neglect of any correlations between the motion of perturbers and radiators is justified. Later, the area of applicability was extended by means of using hyperbolic paths for the perturbers (e.g., see Ref. [17]). In these studies, the time development of the radiator was obtained by using a special technique [18] specific to the hydrogen atom (or hydrogen-like ions) with the $SO(4)$ symmetry. This technique is very advantageous, allowing for a large reduction in the computational time, but evidently, it restricts the use of the model to hydrogen-like systems (with linear Stark effect), and does not account for the fine-structure splitting and for the interactions between eigenstates with different principal quantum numbers. Furthermore, it does not allow for the addition of external magnetic fields.

In order to address the limitations of the existing approaches, we developed a method for line-shape calculations, as discussed in Section 2. In Section 3 described is the application of the method, demonstrating its use in studying various effects in Stark line-broadening and in illuminating the dominant mechanisms for different plasma parameters. The accuracy of the results is also discussed.

2. The calculation method

2.1. The concept

The shape of a spectral line is calculated in three main steps, as depicted in Fig. 1. First, the perturbing fields are simulated by the particle field generator (PFG), where the motion of a finite number of plasma particles (electrons and ions) is calculated assuming that classical trajectories

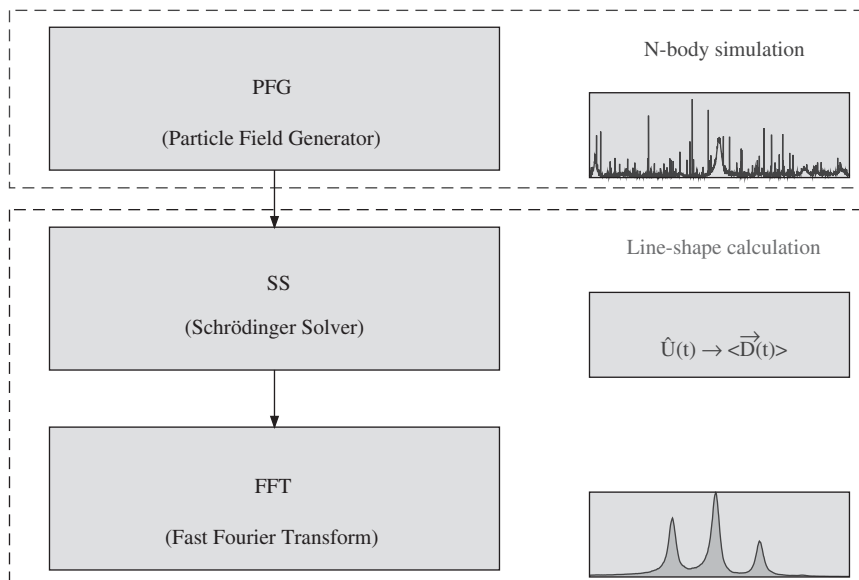


Fig. 1. Schematic diagram of the method.

are valid. Then, using this field as a perturbation, the radiator dipole oscillating function is calculated by the Schrödinger solver (SS). Finally, using the fast Fourier transformation (FFT) method, the power spectrum of the radiator dipole oscillating function is evaluated, giving the spectral line shape. Since the perturbing field, by its very nature, is significantly random, averaging the results of repeated runs of this procedure is then required to obtain a smooth spectrum.

By using the total field perturbation, no a priori separation of the effects of electrons and ions is made, therefore allowing for the slow component of the electron perturbation as well as the fast component of the ion perturbation to be accounted for. The scheme of the present method is thus similar to that of the approaches [13–16] outlined in the previous section. However, here we use a rather general approach for solving the Schrödinger equation (see Section 2.3), thus the atomic systems considered are not restricted to hydrogen-like species. Therefore, the code can be used for the calculation of spectral line broadening of isolated lines as well as transitions in hydrogen-like atomic systems, including intermediate cases that are between the quadratic and linear Stark effects. Furthermore, line-shapes of dipole-forbidden transitions, that are rather difficult to calculate for the intermediate cases, can also be treated accurately. The general approach in the SS also allows for accounting for effects of external electric and magnetic fields in a convenient way. Also, polarization properties of the emitted light, induced by the addition of the external fields (which in general breaks isotropy), can be calculated. In addition, when the interactions between the plasma particles are accounted for (either for the entire particle set, or only a part of them) in the PFG, the correlation effects can be investigated in an ab initio way.

A disadvantage of this method is the considerable computation time (a run may last from minutes to many hours or even days on a modern PC).

2.2. The particle field generator

The particle field generator produces time-dependent histories of the electric field $\vec{F}_p(t)$ and the coordinates $\vec{r}_p(t)$ of the corresponding radiator particles, where the index p corresponds to the p th radiator. It is obtained from a computer simulation of the motion of the plasma particles (both ions and electrons). It is at this point that the effect of “macro” electric and magnetic fields on the line-shape calculations can be taken into account by addition to the particle fields $\vec{F}_p(t)$. Such fields can either represent externally-applied fields or fields that are known to be present due to collective phenomena in the plasma. The addition of such fields to $\vec{F}_p(t)$ in the PFG calculations yields the effect of these fields on the plasma-particle motion, which further modifies the calculated fields. However, in cases when such macro fields are known to be negligible with respect to the motion of the plasma particles, they can be excluded from the PFG calculations and added to the PFG output, thus allowing for the same PFG output to be re-used for several configurations of the external fields.

Simulating the plasma-particle motion and the fields generated by them means solving the N -body problem. The equations of motion of a system of N_p particles (N_p is the total number of the ions and electrons) are described by a set of N_p ordinary differential equations. Given initial positions and velocities, a computer simulation generates all the trajectories by numerical integration. At each time step each particle moves according to its velocity, and then the particle velocity is updated consistent with the force exerted on the particle by the other particles and macro-fields. The initial positions of the particles are set randomly within the volume of the

simulation, and the initial velocities are set randomly according to a Maxwellian distribution corresponding to the temperature assigned to a given type of particles.

The assumption of independent particle positions and velocities is inconsistent with the Gibbs distribution. Therefore, for moderately- or strongly-coupled plasmas, the output of the PFG cannot be used at the initialization of the calculations. Some time is required for the simulated plasma to thermalize. Usually, the time for thermalization is about one average particle-crossing-time for the volume assumed.

The PFG run may be very time-consuming, since, for each time step for each particle, the total force due to the entire set of particles should be calculated, making the calculation time $\sim O(N_p^2)$. However, under certain conditions, a few simplifications can be made that speed up the execution considerably. Such simplifications are discussed below.

2.3. The Schrödinger solver

The Hamiltonian of the atomic system of the radiator is the sum of the unperturbed Hamiltonian H_0 and a time-dependent perturbation V :

$$H = H_0 + V(t), \quad (2)$$

where the perturbation is due to the PFG-simulated plasma electric field and/or the macro-fields.

We try to find a solution for the Schrödinger equation (assuming $\hbar = 1$)

$$i d\Psi(t)/dt = H\Psi(t) \quad (3)$$

by introducing the time-development operator $U(t)$ (acting in the same operator space as H) that gives

$$\Psi(t) = U(t)\Psi_0, \quad (4)$$

where Ψ_0 is a solution of the unperturbed Hamiltonian:

$$i d\Psi_0/dt = H_0\Psi_0. \quad (5)$$

Note that Ψ_0 includes the e^{-iEt} time dependence. Inserting Eq. (4) into Eq. (3) and using Eq. (5) we obtain

$$i dU(t)/dt = [H_0, U(t)] + V(t)U(t), \quad (6)$$

or, in the interaction representation,

$$i d\tilde{U}(t)/dt = V(t)\tilde{U}(t). \quad (7)$$

The time evolution of the dipole operator $D(t)$ is then obtained using the time-development operator:

$$D(t) = U(t)^\dagger D(0)U(t). \quad (8)$$

The Fourier transform of the dipole operator

$$\vec{D}(\omega) = \int_0^\infty dt \exp(-i\omega t)\vec{D}(t) \quad (9)$$

is then used to calculate the line spectrum. In the dipole approximation, the intensity of the emitted light polarized in the \vec{e}_λ direction is given by the following expression:

$$I^\lambda(\omega) = \frac{1}{2\pi} \sum_i \sum_f \omega_{fi}^4 |\vec{e}_\lambda \cdot \langle \vec{D}_{fi}(\omega) \rangle|^2, \quad (10)$$

where the i and f indices run over the initial and final levels, respectively, $\omega_{fi} = E_i - E_f$ is the level-energy difference, and the angle brackets denote an averaging over several runs of the code (which corresponds to an averaging over a statistically-representative ensemble of radiators). Evidently, if the number of radiators used in the PFG run is more than one, the procedure described here is repeated for each of them and then averaged.

The formula above gives the line intensity assuming all the initial levels are equally populated. If this assumption is not used, each initial state i is assigned a population factor ρ_i , giving

$$I^\lambda(\omega) = \frac{1}{2\pi} \sum_i \rho_i \sum_f \omega_{fi}^4 |\vec{e}_\lambda \cdot \langle \vec{D}_{fi}(\omega) \rangle|^2. \quad (11)$$

For a complete calculation of the line shape in the plasma, the Doppler effect should also be incorporated, thus we define

$$\sigma_D(\omega) \equiv \omega \sqrt{\frac{k_B T}{M}}, \quad (12)$$

where M and T are the mass and the temperature of the radiator, respectively, and k_B is the Boltzmann constant. The Doppler-broadened spectrum is then:

$$I_D^\lambda(\omega) = \int_0^\infty \frac{d\omega'}{\sqrt{2\pi\sigma_D^2(\omega)}} I^\lambda(\omega') \exp\left\{-\frac{(\omega - \omega')^2}{2\sigma_D^2(\omega)}\right\}. \quad (13)$$

However, if the velocity distribution of radiators is not Maxwellian, the convolution function in Eq. (13) should be modified accordingly.

Note that Eq. (13) gives the line shapes for each polarization direction. In general, the line shapes may be polarized in the presence of anisotropic electric or magnetic fields in the plasma, or due to different populations of the sublevels corresponding to different projections of the angular momentum of the initial level. Such an initial level alignment can be a result of, e.g., excitation by a polarized laser beam or by electrons or ions that have a preferred direction of motion [19]. Evidently, in the case of opaque plasmas, the line shapes calculated for each polarization should be used in the radiation-transport calculations, to provide the line shape of the light emitted from the plasma. The scattering and absorption of the photons in such a plasma can evidently alter the polarization of the emerging light.

Note also that such an independent evaluation of the Stark and the Doppler effects is only valid if these effects are not correlated. However, there are cases where this assumption may be unjustified (see Section 2.5). Then, the Doppler correction to the Fourier-transformed dipole operator must be taken into account explicitly, i.e., Eq. (9) becomes

$$\vec{D}(\omega) = \int_0^\infty dt \exp\left\{-i\omega\left(t + \frac{r_{\parallel}(t)}{c}\right)\right\} \vec{D}(t), \quad (14)$$

where $r_{\parallel}(t)$ is the line-of-sight projection of the (time-dependent) radius-vector of the given radiator particle, as produced, along with the fields at that radiator, by the PFG (see Section 2.2). The rest of the calculation procedure remains unmodified as outlined above, however, in this case Eq. (10) or (11) give the line shape in which included are both the Stark and the Doppler effects, and any correlations between them. We note that Eq. (14) accounts for correlations between the Stark and Doppler effects both on the short (collision duration) and long time scales. When only the latter is important (e.g., for neutral radiators), the correlation effect can be modeled using the μ^* approach [20].

2.4. Computation accuracy and time scales

In order not to miss an important feature in the electric-field history, the time step of a PFG run should be significantly smaller than the typical time scale of the change in the field due to the motion of the fastest particles (usually electrons), i.e., $\Delta t \ll v_e/\rho$, where v_e is the electron velocity and ρ is the average inter-particle distance. The total simulation time t should be long enough to collect a representative statistics of the quasistatic field distribution, thus it should allow the slowest particles (usually ions) to cross the inter-particle distance several times, i.e., $t \gg v_i/\rho$.

Since the final line shape is produced by performing a Fourier transform, the total simulation time should be sufficiently long to provide the required accuracy $\delta\omega$ in the line shapes, i.e., it is required that $t \gg (\delta\omega)^{-1}$. This is probably the most challenging requirement, especially since the relative accuracy $\varepsilon_\omega = \delta\omega/w$ depends on the final line width w that is not known a priori. This requires that the calculation be iterative. Similarly, if there is an interest in the shapes of the line far wings, the computation time step Δt should be small enough to cover a broad range of frequencies, i.e., it is required that $\Delta t \ll \Omega^{-1}$, where Ω is the frequency difference from the unperturbed line center. The later requirement is actually rather weak and is easily satisfied.

Since it is required to average the line-shape calculations over several runs, the total time of the simulation of the plasma-particle motion by the PFG is divided between the runs. Therefore, for each of N_r runs only $t_r = t/N_r$ is used (we note that this procedure reduces the overhead due to the thermalization time since this time needs to be skipped only once). Thus, the spectral uncertainty introduced by the FFT, as argued above, is N_r/wt . On the other hand, the relative error ε_A introduced by the statistical noise (that is reduced by the averaging) is proportional to $1/\sqrt{N_r}$. Combining these arguments, one finds that

$$\varepsilon_\omega \varepsilon_A^2 \sim 1/wt. \quad (15)$$

Here, the actual value of the proportionality coefficient is specific for a given transition for a given set of plasma parameters; however, in general, it is of the order of a unity. Evidently, the overall numerical accuracy ε_{num} of the line shape is limited by the largest of the ε_ω and ε_A uncertainties. Therefore, for a given t , because of the constraint given by Eq. (15), the most accurate results are achieved when $\varepsilon_\omega = \varepsilon_A$. Thus, we obtain that

$$t \sim (w\varepsilon_{\text{num}}^3)^{-1}. \quad (16)$$

We note that the strong dependence of the total simulation time on the accuracy desired is directly translated to the computational resources.

2.5. Implementation details

Since the PFG is a time-consuming part of the calculations, it is a separate computational code that runs independently of the rest of the calculations. This allows the PFG output to be used for several runs of the line shape calculations, i.e., for different spectral lines of the same or even different species. Furthermore, this separation allows for the use of electric-field simulations other than the present one, e.g., an output of a particle-in-cell (PIC) code, with no need to modify the line shape calculation module.

In order to reduce PFG runtime, a few simplifications justified under certain conditions can be made. The most radical is to avoid the calculation of the interaction between the particles, thus allowing them to move along straight paths, but for the field evaluation, to approximate the correlation effects by introducing the effective Debye-screened potential. The motion of the radiators is not considered, however assigning the reduced mass to the perturbers compensates for that. This is the approach used, e.g., in the calculations in Ref. [16]. Such an approximation neglecting the interactions between the radiators and other particles is justified for neutral or low-charge radiators in weakly coupled plasmas.

For the line-shape calculations presented in this study, we used another approximation in the PFG, unless otherwise indicated. Here, the motion of the radiators is neglected and the interactions between the perturbers is taken into account by assigning an effective Debye-screened potential to them. However, the radiator–perturber interactions (RPI) are taken into account rigorously, hence resulting in curved trajectories for the perturbers. In this scheme, the Debye potential is also assigned to the radiator, therefore the trajectories of the perturbers are not hyperbolic. To summarize: each perturbing particle has a Debye potential with an effective Debye length for a species s , calculated under the assumption that species heavier than s do not contribute to the screening, i.e.,

$$\lambda_s = \left(\sum_{m_{s'} \leq m_s} \frac{4\pi n_{s'} e^2 Z_{s'}^2}{k_B T_{s'}} \right)^{-1/2}, \quad (17)$$

where $m_{s'}$, $n_{s'}$, $Z_{s'}$, and $T_{s'}$ are, respectively, the mass, the density, the charge, and the temperature of species s' . The Debye potential is used to calculate the electric field acting on a radiator residing at the center of the simulation volume, taken to be spherical. The radius of the simulation volume, a , should be at least a few times the largest Debye length (which is the electron Debye length λ_e), i.e., $a \gg \lambda_e$. The motion of the perturbers is affected by the radiator static electric field, which is evaluated assuming the Debye screening according to Eq. (17). This reduces the complexity of the N-body calculations to $O(N_p)$, while preserving the important effects of particle interactions on the electric-field distribution. The use of this approach is justified for cases when there is a small fraction of highly-charged, heavy radiators embedded in plasma of low-charge light ions. The requirement that radiator density should be lower than the perturber density is needed since the typical distances at which the ion perturbers affect a given radiator are (unless approaching the impact limit) comparable to the inter-particle distances. The radiator charge must be significantly larger than that of other ions for the influence of the radiator on the perturber to be dominant. Also, the radiator is required to be heavier than the perturbers since otherwise the recoil effect will be substantial, resulting in a strong coupling between the Stark effect and the kinetic motion

of the radiator, thus making the independent treatment of the Doppler effect using Eq. (13) inapplicable.

At the start of a simulation, each particle is assigned an initial kinetic energy according to the Maxwellian distribution of velocities, as explained in Section 2.2. When a particle exits the simulation volume, it is injected back at a random point on the sphere with the initial energy, thus the numerical errors in the MD process are not accumulated. This also eliminates the heating of the simulated plasma due to the initial thermalization. Evidently, the re-injection procedure introduces a noise in the simulated electric field, which can be reduced by choosing a sufficiently large number of particles so that the boundary effects become negligible. The use of the Debye potential, rapidly falling off beyond the Debye length, allows for the use of a smaller number of particles than that required in analogous true Coulomb MD calculations. The quality of the simulation is examined by varying the number of particles and verifying that a good convergence occurs both for the distribution of the microfield amplitudes and the distribution of their time derivatives.

The method described in Section 2.3 is applicable for any choice of the eigenstate basis and the unperturbed Hamiltonian. However, from the practical point of view, it is important to choose a convenient basis. We selected the n, l, m_l, m_s representation and used the LS approximation. This choice enabled us to apply the method to a large variety of atomic species, both for cases where the LS interaction is important and when it can be neglected. In the latter case, the respective perturbation term can be simply omitted, giving a two-fold reduction of the number of states and, hence, a significant reduction of the computation time (see below).

Based on this discussion, H_0 is diagonal and corresponds to eigenvalues of the energy levels without the LS-interaction, while the perturbation part V is of the form

$$V = V_{\text{LS}} + V_{\text{EF}} + V_{\text{MF}}, \quad (18)$$

where V_{LS} is the perturbation due to the LS-coupling, V_{EF} is the electric field perturbation (which includes the perturbation due to the plasma particles and possible external electric fields), and V_{MF} is the perturbation due to the magnetic field. Here,

$$V_{\text{LS}} = A_{nl} \vec{l} \cdot \vec{s}, \quad (19)$$

where \vec{l} and \vec{s} are, respectively, the total electron angular momentum and spin, and A_{nl} are constants derived from the atomic level data tables. The perturbation caused by the total electric field is

$$V_{\text{EF}} = -e\vec{F} \cdot \vec{r}, \quad (20)$$

where \vec{F} is the electric field and \vec{r} is the radius-vector of the optical electron, and that caused by the external magnetic field is

$$V_{\text{MF}} = \mu\vec{B} \cdot (\vec{l} + 2g_e\vec{s}). \quad (21)$$

Here, μ is the Bohr magneton and g_e is the electron g -factor. The matrix elements of the perturbation terms (19)–(21) are given in Ref. [21].

Since the calculation time is proportional to N_{st}^3 , where N_{st} is the number of states in the Hamiltonian, it is desirable to examine ways to limit the number of states used, without affecting the calculation accuracy. For example, for spectral lines where the effect of high-lying discrete and

continuum states can be considerable, it is possible to replace them with a few “effective” levels, e.g., see Ref. [21]. Such a procedure is justified for states that have sufficiently large energy separation from the initial and final states of the radiative transition so that the Stark effect due to these states is quadratic.

3. Results and discussion

We present a few examples for line shapes of H- and He-like ions of carbon, silicon, and argon. In several cases, we compare results obtained using the new method with those calculated according to the ST. The ST calculations were performed by first evaluating the quasistatic line broadening and then applying a convolution with the broadening obtained by running the PFG with only electrons. This corresponds to the assumption that the impact operator ϕ in Eq. (1) does not depend on the ion field F . This assumption is broadly correct, as discussed in Ref. [22]; the inaccuracy introduced by this approximation is irrelevant to the comparisons presented here. The effect of the radiator–perturber interactions (RPI) is demonstrated in several examples by providing the line shapes calculated with and without the RPI taken into account.

For the calculations described below, the total number of particles in the PFG runs was 2000, satisfying the criteria outlined in Section 2.5. Because the radiators considered in the calculations are near-degenerate atomic systems, we did not include in the Hamiltonian states other than those of the same principal quantum number as the initial or the final levels of the radiator (see Section 3.4). Also, we assumed no magnetic field, thus the V_{MF} perturbation term in Eq. (18) is omitted. Finally, for the spectra presented the convolution with the Doppler broadenings is not made. However, for comparison, the Doppler full-width-at-half-maximum (FWHM) values are quoted in the figure captions.

3.1. Carbon-line spectra

All calculations presented in this subsection were performed for a CH_4 plasma with $n_e = 10^{21} \text{ cm}^{-3}$ and $T_e = T_i = 100 \text{ eV}$. In a steady state at these conditions, the hydrogen is fully ionized and the mean charge state of carbon is ~ 5 . Therefore, in the PFG simulation we used a proportion of 9:4:1 for the electrons, protons, and C^{5+} , respectively.

In Fig. 2, the C VI Ly_α profile is presented, together with the line shape obtained from the ST calculations, showing the two narrow components that are due to the fine-structure V_{LS} term in Eq. (18) (in the presence of the dominating quasistatic Stark effect, the splitting and the intensities are different from those of the fine-structure components in the zero-field limit). The strong contribution of the ion dynamics is clearly seen; the line broadening obtained is almost 6 times larger than that resulting from the ST calculations.

Fig. 3, giving the C VI Ly_β profile, in comparison to the ST calculations, shows the anticipated effect of the ion dynamics on the Lyman transitions that have no central component, which is a filling in the central minimum of the line profile.

In order to examine the effect of the RPI on the line shapes, calculations were performed in which no RPI was included. For the carbon-ion lines it was found that the RPI effects cause a reduction of a few percent in the line widths. The reason for the reduction is that the RPI causes a

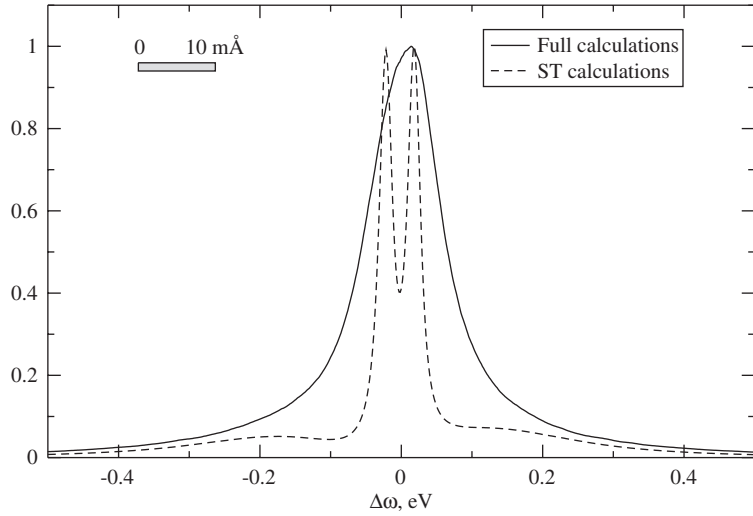


Fig. 2. The C VI Ly_α Stark profile in a CH₄ plasma with a total $n_e = 10^{21} \text{ cm}^{-3}$ and $T_e = T_i = 100 \text{ eV}$. The Doppler FWHM is 0.082 eV (not accounted for in all line shapes presented in this paper).

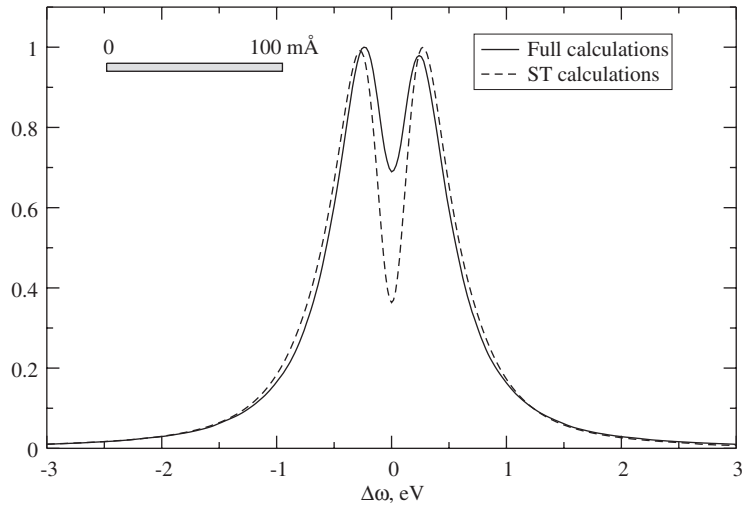


Fig. 3. The C VI Ly_β Stark profile. The plasma conditions assumed are the same as in Fig. 2. The Doppler FWHM is 0.097 eV.

repulsion between the radiator and the plasma ions, resulting in weaker electric fields due to the ion perturbers. The effect of the RPI on the perturbation caused by the electrons is of the opposite sign. Furthermore, in the impact limit, the effect vanishes in the first order since the effect of the stronger electric field (due to the attraction of the perturbing electron to the radiator) is compensated for by the shorter duration of the given collision (due to the higher electron

velocity). Since the effect of the RPI is small for the spectral lines discussed above, we do not provide the line shapes calculated with the RPI omitted.

We note that the presence of the heavy and highly-charged carbon ions in the plasma could, in principle, violate the conditions required for the approximation used to generate the plasma fields. However, the fraction of the carbon ions is relatively low and they contribute a minor part of the total line broadening. To confirm this we performed a plasma field generation using a true N-body molecular-dynamics code with periodic boundary conditions [23] that resulted in line widths that agree within a few percent with those presented (the total number of particles in this simulation was 1260).

3.2. Silicon-line spectra

The calculations presented in this subsection, unless mentioned differently, are for Si H- and He-like ions embedded as a minority in a CH₂ plasma with $n_e = 10^{22} \text{ cm}^{-3}$ and $T_e = T_i = 500 \text{ eV}$. In steady state, all hydrogen and most of the carbon are fully ionized leading to a plasma with a proportion 8:2:1 of electrons, protons, and carbon, respectively.

The calculated line shape for Si xiv Ly_α is given in Fig. 4 together with a profile based on the ST calculations and one obtained when the RPI effects are not accounted for. The comparison of the full-calculation and the ST profiles demonstrates that the ion-dynamics effects produce widths for the two fine-structure components that are several times larger than when the ion motion is neglected. Further, the effect of the RPI causes a reduction of the Ly_{α1} and Ly_{α2} Stark widths by ≈ 30% and 15%, respectively.

An interesting effect is the different widths (and, in general, shapes) of the two components of this transition. This is due to the different polarizabilities of the 2p_{1/2} and 2p_{3/2} levels (the 2p_{1/2}

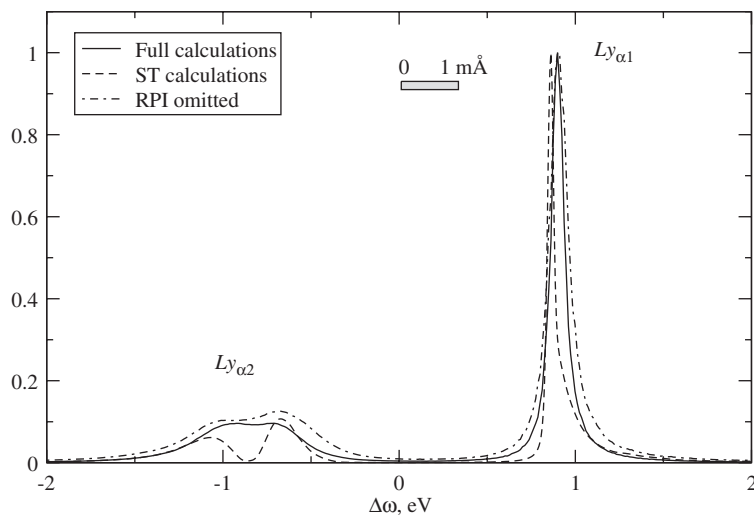


Fig. 4. The Si xiv Ly_α Stark profile for a silicon minority in a CH₂ plasma with a total $n_e = 10^{22} \text{ cm}^{-3}$ and $T_e = T_i = 500 \text{ eV}$. The Ly_{α1} and Ly_{α2} components are seen. The zero energy corresponds to a weighted average of the Si xiv $n = 2$ levels. The Doppler FWHM is 0.65 eV.

level lies very close to the $2s_{1/2}$ level), causing the width of the $\text{Ly}_{\alpha 2}$ ($1s_{1/2}-2p_{1/2}, 2s_{1/2}$) component to be much larger than that of $\text{Ly}_{\alpha 1}$ ($1s_{1/2}-2p_{3/2}$). In fact, such a difference can be important because, although the $\text{Ly}_{\alpha 1}$ Stark width is negligible compared to the Doppler broadening, the $\text{Ly}_{\alpha 2}$ width is comparable to it. While possibly difficult to observe directly due to the opacity effects, such an anomaly may be important for the plasma radiation transport.

In a sense, the two components of the Ly_{α} line exhibit features usually found in different transitions. The $\text{Ly}_{\alpha 1}$ component depends on the electric field quadratically and its shape resembles that of an isolated line (albeit with a rather large broadening due to the close $2s_{1/2}$ level). On the other hand, the $\text{Ly}_{\alpha 2}$ component has an almost linear Stark effect and due to the absence of the central component, it demonstrates two peaks separated by the central dip. The separation of two peaks appears to be similar to Ly_{β} ; however, due to the finite Lamb shift, one of its two “sub-components” ($1s_{1/2}-2s_{1/2}$) is, in fact, a dipole-forbidden transition for low values of the plasma electric field. This explains the $\text{Ly}_{\alpha 2}$ asymmetry. The asymmetry in the shape of $\text{Ly}_{\alpha 1}$, that is seen in the ST calculations, is due to the different polarizabilities of states corresponding to different projections of the angular momentum of the $2p_{3/2}$ level ($|m_j| = \frac{1}{2}$ and $\frac{3}{2}$). For $|m_j| = \frac{3}{2}$, the quadratic Stark effect is exactly zero if the interactions with $n \neq 2$ levels are neglected. This asymmetry is mostly smeared out by the ion-dynamics effect.

In Fig. 5, we present the Si xiv Ly_{β} profiles calculated for different electron temperatures, which provides an examination of the effect of the electron screening. As expected, for higher electron temperatures the screening is weaker, resulting in somewhat stronger plasma electric fields and, as a result, in slightly wider line profiles. The broadening due to the electron-impact effect, however, although rather weak for the Ly_{β} line, tends to be slightly larger for lower temperatures. The resultant effect is a little wider line for higher electron temperatures.

We note that, in general, the screening should not only be understood in the static meaning (as merely reducing the average electric field strength), since the screening also causes the spectrum of the perturbing fields to shift to higher frequencies. This results from the fact that perturbers with

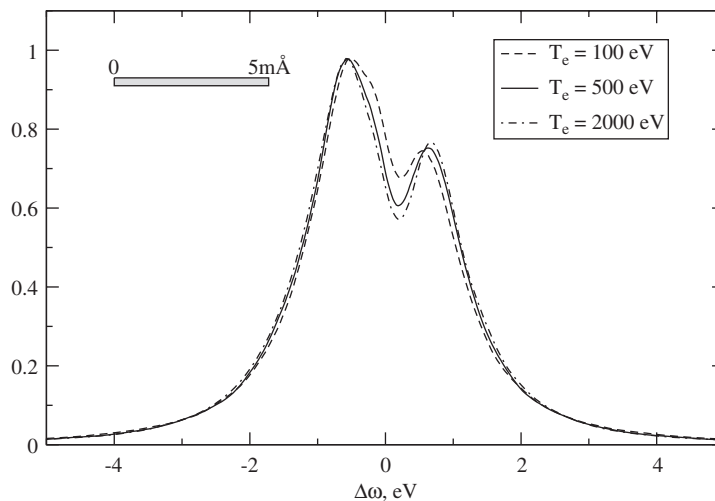


Fig. 5. The Si xiv Ly_{β} Stark profile as a function of the electron temperature. Except for the electron temperature, the plasma conditions assumed are the same as in Fig. 4. The Doppler FWHM is 0.77 eV.

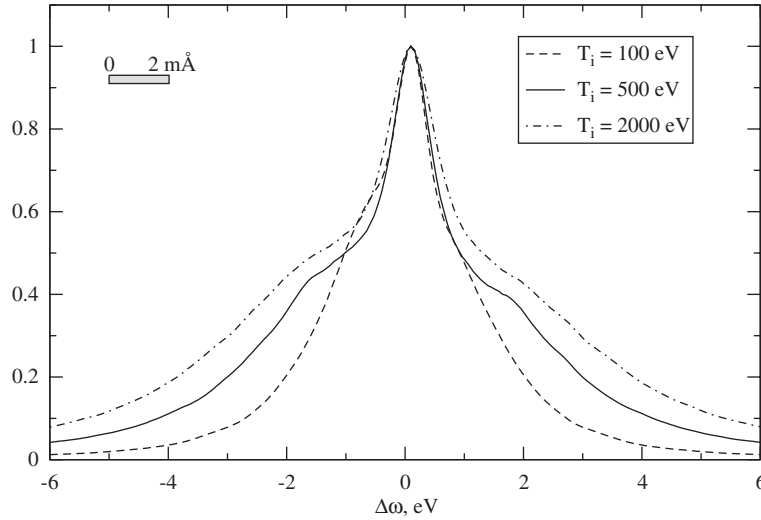


Fig. 6. The Si XIV Ly $_{\gamma}$ Stark profile as a function of the ion temperature. Except for the ion temperature, the plasma conditions assumed are the same as in Fig. 4. The Doppler FWHM for $T_i = 500$ eV is 0.82 eV.

small impact parameters (responsible for the high frequencies of the field spectrum) are screened less than larger-impact-parameter perturbers.

In Fig. 6, we present the Si XIV Ly $_{\gamma}$ profiles calculated for different ion temperatures. It is seen in Fig. 6 that higher ion temperatures correspond to wider line profiles, confirming the dominance of the ion broadening in the line widths. For low ion temperatures, the core of the spectral line tends to approach the electron-impact shape, while the wings become strongly affected by the RPI. We note that the dependence of the shapes of the line wings on the ion temperature is mainly due to the corresponding change in the quasistatic microfield distribution when the ion–ion correlation effects are accounted for [24].

In order to demonstrate the influence of the plasma composition on the line shapes, we performed calculations of the Si XIV Ly $_{\epsilon}$ profiles for C, CH $_2$, and H plasmas with n_e and T kept constant, as shown in Fig. 7. It is seen that the protons produce larger line broadening. In principle, this could result from the weaker RPI for the proton perturbers due to their smaller charge, which tends to lead to broader lines. However, by comparing calculations with and without the RPI, it was verified that the role of the RPI effect in this case is relatively small and that the larger broadening for protons results from their high velocities, as expected from the dominance of the ion dynamics. Note that this is despite the fact that the average electric field due to the plasma ions is smaller for the case of a proton plasma (since the Holtsmark field constant is proportional to $Z_{\text{ion}}^{1/3}$ for a constant n_e). This further confirms the dynamic nature of the ion-broadening effect.

He-like ions provide a convenient example for investigation of dipole-forbidden transitions. In Fig. 8 we present the Si XIII He $_{\beta}$ transition including its two dipole-forbidden components, that correspond to the $1s^2(^1S)–1s3d(^1D)$ and $1s^2(^1S)–1s3s(^1S)$ transitions. In fact, for the plasma parameters here discussed, the $1s3d(^1D)$ and $1s3p(^1P)$ levels are mixed rather strongly by the

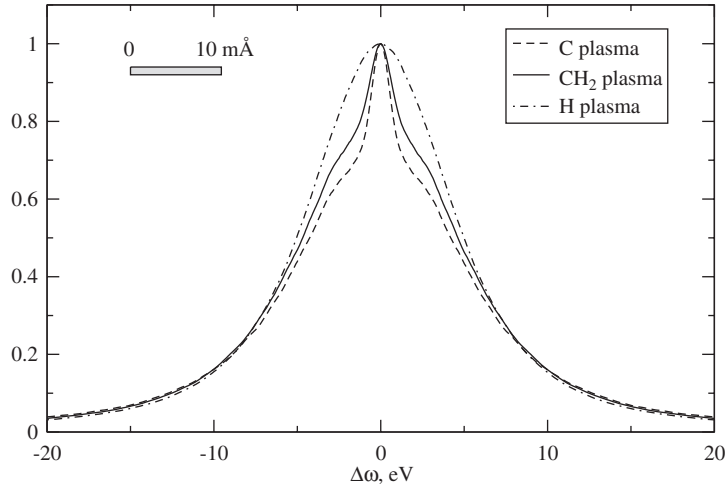


Fig. 7. The Si XIV Ly_ε Stark profile, calculated for different plasma compositions. The other plasma parameters are the same as in Fig. 4. The Doppler FWHM is 0.84 eV.

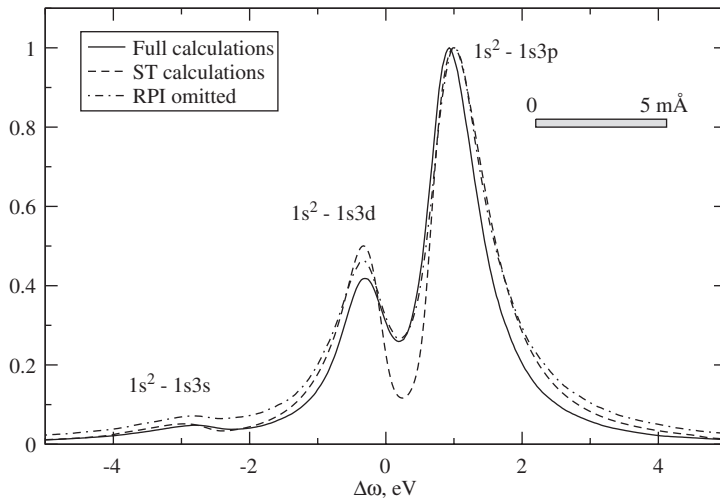


Fig. 8. The Si XIII He_β Stark profile, including its two dipole-forbidden components. The plasma conditions assumed are the same as in Fig. 4. The zero energy corresponds to a weighted average of the Si XIII 1s l levels. The Doppler FWHM is 0.71 eV.

plasma fields, thus the intensity of the $1s^2(^1S)–1s3d(^1D)$ transition acquires a substantial fraction of the $1s^2(^1S)–1s3p(^1P)$ allowed line. On the other hand, the $1s^2(^1S)–1s3s(^1S)$ transition remains weak. Note the significant modification of the dip separating the forbidden $1s^2(^1S)–1s3d(^1D)$ and the allowed line components due to the ion-dynamics effect. Also, the reduction of the line width caused by the RPI is not negligible ($\approx 10\%$).

3.3. Argon-line spectra

Here is further investigated the influence of the radiator–perturber interactions on line shapes. In Fig. 9 the results of calculations for the Ar xvii He $_{\alpha}$ transition in a hot and dense deuterium plasma are shown. Here the RPI effects cause about 35% reduction in the line-width. Similar calculations performed for the Ar xvii He $_{\beta}$ transition, presented in Fig. 10, show a smaller line-width reduction. The latter can be explained by the fact that the repulsion between the radiator and the perturber ions not only results in the reduction of the effective field, but also in the

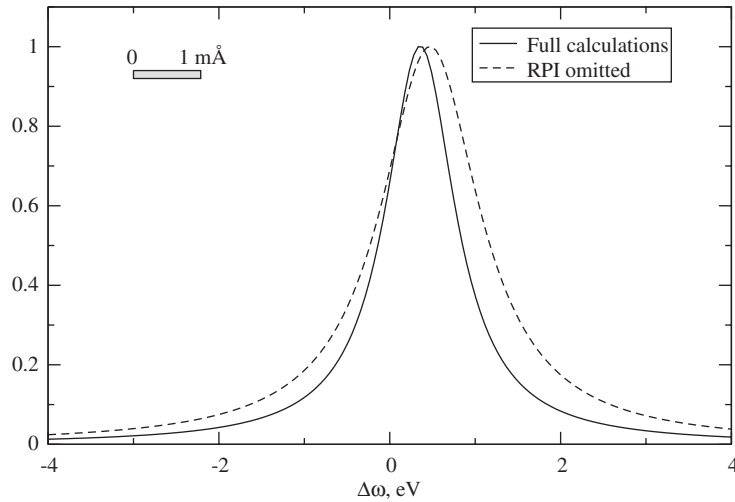


Fig. 9. The Ar xvii He $_{\alpha}$ Stark profile for argon ions as a minority in a deuterium plasma with a total $n_e = 5 \times 10^{23} \text{ cm}^{-3}$ and $T_e = T_i = 900 \text{ eV}$. The Doppler FWHM is 1.1 eV.

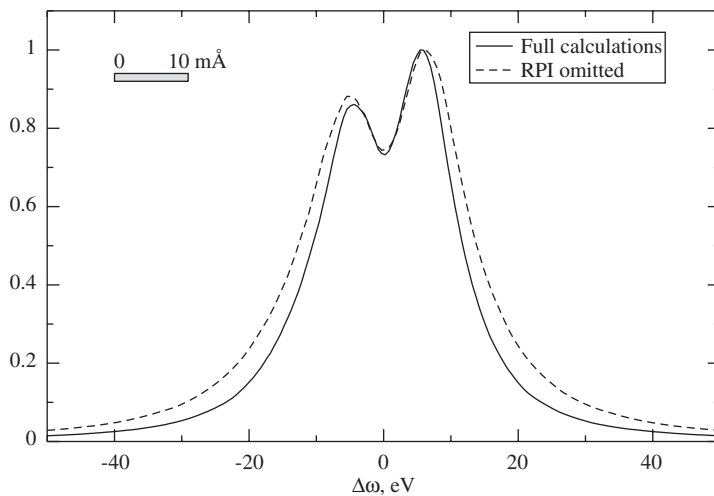


Fig. 10. The Ar xvii He $_{\beta}$ Stark profile for the same plasma conditions as in Fig. 9. The Doppler FWHM is 1.3 eV.

enhancement of the slow components of the plasma field. This is because the distances of the closest approach of the perturbing ions become larger and the velocities of the perturbing particles in the interaction region become lower. This effect of the RPI on the spectrum of the perturbation is less noticeable in the case of He_β , since it has no central component and, thus, its width is less sensitive to the ion-dynamics effects.

Another reason for the larger sensitivity of the He_α shape to the RPI effects is that the Stark effect of the Ar xvii He_α transition is mainly quadratic for the typical fields for these plasma parameters. We note the similar effect in the case of the two components of the Si xiv Ly_α line (see Section 3.2), where the $\text{Ly}_{\alpha 1}$ component showed a stronger influence of the RPI effect than the $\text{Ly}_{\alpha 2}$ “beta-like” component.

It is of interest to discuss the plasma coupling parameter, Γ , defined as the ratio between the electrostatic (Coulomb) energy to the thermal energy of plasma, i.e., $\Gamma = E^{(C)}/E^{(\text{Th})}$. It is evident that plasma coupling results in the correlation of the motion of the Coulomb-interacting plasma particles whose trajectories are no longer straight lines. Therefore, Γ may serve as a measure of the modifications of the plasma fields due to the interactions between the plasma particles. However, for multi-component plasmas, such an average value is not a sufficient criterion. Thus, we introduce the “cross-coupling” matrix, which reflects the extent that the motion of a particle of the species s is affected by the potential field of particles of another species s' :

$$\Gamma_{s,s'} = E_{s,s'}^{(C)}/E_s^{(\text{Th})}. \quad (22)$$

Here, $E_s^{(\text{Th})} \equiv \frac{3}{2}k_B T_s$ and $E_{s,s'}^{(C)}$ is

$$E_{s,s'}^{(C)} = Z_s Z_{s'} e^2 \langle r_{s,s'}^{-1} \rangle, \quad (23)$$

where $r_{s,s'}$ is a distance between a particle of the species s and its nearest neighbor of the species s' , and the averaging, denoted by the angle brackets, is performed over all particles of these two species. The diagonal elements of the $\langle r_{s,s'}^{-1} \rangle$ matrix can be estimated as $n_s^{1/3}$, while the off-diagonal ones, for the case of s' being a dopant (i.e., $n_{s'} \ll n_s$), as $2n_s^{1/3}$.

A particular element of the $\Gamma_{s,s'}$ matrix can be large even when the total Γ is small. This is the case for the deuterium plasma discussed. Indeed, despite the rather high total electron density, the plasma is overall weakly-coupled, because of the small charge of the deuterons and the negligibly-low density of the argon ions, giving $\Gamma \simeq 0.01$. However, for the problem addressed in this study, the question of interest is the effect of the charged radiator on the trajectories of the perturbing ions. The coupling parameter $\Gamma_{d,\text{Ar}^{+16}}$ can thus be used as a measure of the effect of the potential field of the Ar^{+16} ions on the motion of deuterons close to those ions. For the present plasma parameters, the value of this parameter is about 0.27. Indeed, the corrections to the line widths of the argon ions due to the RPI effect are of the same magnitude.

Similar considerations apply to the case of the Si xiv broadening given in the previous subsection. For those plasma conditions, one finds a small cross-coupling parameter for protons ($\Gamma_{p,\text{Si}^{+13}} \approx 0.07$) and a large one for the carbon ions ($\Gamma_{\text{C}^{+6},\text{Si}^{+13}} \approx 0.32$). Although the cross-coupling parameter for the carbon ions is large, the relatively small fraction of the carbon in the plasma (1/3) makes the net coupling parameter for the carbon-ions and protons rather low, causing the effect of the RPI somewhat less pronounced than in the case of the argon line shapes discussed above. Finally, for the plasma parameters used for the calculations of the carbon lines

given in Section 3.1, one obtains $\Gamma_{p,C^{+5}} \approx 0.07$ and $\Gamma_{C^{+5},C^{+5}} \approx 0.11$, which explains the small RPI effect for those lines.

3.4. The accuracy of the results

Several factors contribute to the total error in the line shape calculations. In addition to the numerical factors addressed in Section 2.4, there are inaccuracies that are caused by assumptions concerning the classical-path trajectories for the plasma particles and ignoring the higher-than-dipole multipole interactions. Further, approximations were specifically employed for these calculations, namely, the use of the Debye–Hückel potential and the inclusion in the Hamiltonian only states of the same principal quantum number as that of the initial or final levels. The contribution of each of these inaccuracies for the cases discussed does not exceed a few percent, and, in addition, they partially cancel each other. Due to the complexity of the problem a rigorous evaluation of the total error is infeasible. However, it is our belief, based on various examinations, that the line widths obtained from the line shapes here presented are accurate to within $\lesssim 15\%$, of which the numerical errors, as estimated by Eq. (16), contribute $< 5\%$.

Let us make a special note regarding the justification of the use of the classical-path trajectories for the evaluation of the perturbation. In general, such a semiclassical treatment of the particles is only valid in cases when the typical size r_{int} of the region of the interaction between the radiator and the perturber significantly exceeds the de Broglie length of the perturber. Estimating r_{int} by $\sqrt{\sigma_{\text{int}}}$, where σ_{int} is the typical cross-section of atomic processes of the radiator involving the initial or the final states of the given spectral transition, this means:

$$\sqrt{\sigma_{\text{int}} m_p k_B T_p} \gg 1, \quad (24)$$

where m_p and T_p are the mass and the temperature of the perturber, respectively. In certain cases this inequality is violated for electrons so that one must treat a subset of the electron collisions, i.e., the “strong collisions”, in a special manner. This usually involves semi-empirical approaches, e.g. see Ref. [25], for choosing a minimal impact parameter for the collisions or the use of fully-quantum-mechanical calculations, e.g. see Ref. [26]. However, in the case of He- and H-like transitions, where the cross-sections of $\Delta n = 0$ transitions are large, the strong collisions contribute little. This is especially true for transitions that are mainly broadened by the ion effects, since the ions, due to their large mass, can almost always be treated semiclassically. We also note that a part of the strong-collision issues concerning divergence of perturbative expansions is irrelevant here since the present approach is non-perturbative.

4. Conclusions

A new method for the calculation of the shapes of dipole-allowed and dipole-forbidden lines involving degenerate, partially-degenerate, and non-degenerate atomic levels in plasma has been developed and implemented. It allows for accounting for the ion-dynamics effects in a fully consistent manner and for treating the effects due to the radiator–perturber interactions. This method can also be used for convenient calculations of line shapes under a simultaneous influence of external electric and magnetic fields. The method was applied to spectral lines of H- and He-like

ions of various species. It was found that the ion dynamics contributes substantially to the line broadening for a subset of the cases studied and in several cases exceeds the electron impact widths by a few times. It was also shown that for non-ideal plasmas the correlation effects due to the radiator–perturber interactions affect the line broadening significantly. The cases presented were selected to demonstrate the various aspects involved in line-shape calculations. The variety of line shapes is caused by the interplay between the several mechanisms of the Stark effect, and is further complicated by deviations of the atomic-level energies from the pure degenerate limit.

Acknowledgements

It is with great pleasure that we thank H.R. Griem for invaluable suggestions and for sharing with us his deep insight throughout the entire work. We are indebted to S. Alexiou for highly valuable discussions and reading the manuscript. A thorough editorial work of R.W. Lee has greatly enhanced the quality of the presentation. We are grateful to I.R. Almieiev for his interest and assistance and to S.A. Gurvitz for highly critical comments. The help of D.V. Fisher in running his molecular-dynamics code is highly appreciated.

This work was supported by the German–Israeli Project Cooperation Foundation (DIP), Minerva Foundation (Germany), Israel Science Foundation, and US–Israel Binational Science Foundation.

References

- [1] Griem HR. Principles of plasma spectroscopy. Cambridge: Cambridge University Press; 1997.
- [2] Griem HR. Plasma spectroscopy. New York: McGraw-Hill; 1964.
- [3] Baranger M. In: Bates DR, editor. Atomic and molecular processes. New York: Academic Press; 1962 [chapter 13].
- [4] Cooper J. Rev Mod Phys 1967;39:167.
- [5] Alexiou S. Phys Rev Lett 1996;76:1836.
- [6] Dufty JW. Phys Rev 1969;187:305;
Dufty JW. Phys Rev A 1970;2:534.
- [7] Frisch U, Brissaud A. JQSRT 1971;11:1753.
- [8] Kelleher DE, Wiese WL. Phys Rev Lett 1973;31:1431.
- [9] Grützmacher K, Wende B. Phys Rev A 1977;16:243.
- [10] Grützmacher K, Wende B. Phys Rev A 1978;18:2140.
- [11] Stamm R, Smith EW, Talin B. Phys Rev A 1983;30:2039.
- [12] Stamm R, Talin B, Pollock EL, Iglesias CA. Phys Rev A 1986;34:4144.
- [13] Gigosos MA, Cardenoso V. J Phys B 1987;20:6006.
- [14] Hegerfeld GC, Kesting V. Phys Rev A 1988;37:1488.
- [15] Cardenoso V, Gigosos MA. Phys Rev A 1989;39:5258.
- [16] Gigosos MA, Cardenoso V. J Phys B 1996;29:4795.
- [17] Alexiou S, Calisti A, Gauthier P, Klein L, Leboucher-Dalimier E, Lee RW, Stamm R, Talin B. JQSRT 1997;58:399.
- [18] Gigosos MA, Fraile J, Torres F. Phys Rev A 1985;31:3509.
- [19] Stambulchik E, Maron Y, Bailey JE, Cuneo ME. Phys Rev A 2002;65:052726 and references therein.
- [20] Kesting V. In: Stamm R, Talin B, editors. Spectral line shapes, New York: Nova Science Publishers; 1993. p. 103 and references therein.

- [21] Stambulchik E, Maron Y. *Phys Rev A* 1997;56:2713.
- [22] Griem HR. *Spectral line broadening by plasmas*. New York: Academic Press; 1974.
- [23] Fisher DV, Maron Y. *Eur Phys J D* 2001;14:349;
Fisher DV. *J Phys B* 2003;36:4107.
- [24] Dufty JW, Boerker DB, Iglesias CA. *Phys Rev A* 1985;31:1681.
- [25] Alexiou S. *Phys Rev Lett* 1995;75:3406 and references therein.
- [26] Griem HR, Ralchenko YuV. *JQSRT* 2000;65:287.